

Dynamics of Forced Nucleosome Unraveling and Role of Nonuniform Histone-DNA Interactions

Irina V. Dobrovolskaia and Gaurav Arya*

Department of NanoEngineering, University of California at San Diego, La Jolla, California

ABSTRACT A coarse-grained model of the nucleosome is introduced to investigate the dynamics of force-induced unwrapping of DNA from histone octamers. In this model, the DNA is treated as a charged, discrete worm-like chain, and the octamer is treated as a rigid cylinder carrying a positively charged superhelical groove that accommodates 1.7 turns of DNA. The groove charges are parameterized to reproduce the nonuniform histone/DNA interaction free energy profile and the loading rate-dependent unwrapping forces, both obtained from single-molecule experiments. Brownian dynamics simulations of the model under constant loading conditions reveal that nucleosome unraveling occurs in three distinct stages. At small extensions, the flanking DNA exhibits rapid unwrapping-rewrapping (breathing) dynamics and the octamer flips $\sim 180^\circ$ and moves toward the pulling axis. At intermediate extensions, the outer turn of DNA unwraps gradually and the octamer swivels about the taut linkers and flips a further $\sim 90^\circ$ to orient its superhelical axis almost parallel to the pulling axis. At large extensions, a portion of the inner turn unwraps abruptly with a notable rip in the force-extension plot and a $>90^\circ$ flip of the octamer. The remaining inner turn unwraps reversibly to leave a small portion of DNA attached to the octamer despite extended pulling. Our simulations further reveal that the nonuniform histone/DNA interactions in canonical nucleosomes serve to: stabilize the inner turn against unraveling while enhancing the breathing dynamics of the nucleosome and prevent dissociation of the octamer from the DNA while facilitating its mobility along the DNA. Thus, the modulation of the histone/DNA interactions could constitute one possible mechanism for regulating the accessibility of the nucleosome-wound DNA sequences.

INTRODUCTION

Nucleosomes represent the basic repeating unit of chromatin and consist of 146 bp of DNA wrapped ~ 1.7 times around an octamer of the histones H2A, H2B, H3, and H4 (1,2). Individual nucleosomes are separated by naked portions of DNA called linkers. The resulting chain of nucleosomes folds into the chromatin fiber, which then folds into chromosomes (3). That linkers are 30–80 bp long, depending on the organism and cell type (4), implies that more than two-thirds of the eukaryotic genome is sterically occluded by histone octamers. Thus, nucleosomes present the biggest obstacle to DNA-binding proteins for accessing DNA sequences.

How then do these nucleosome-wrapped DNA sequences get accessed by transcription factors and other DNA-binding proteins? Several mechanisms have been identified that facilitate the accessibility of such wrapped DNA. One mechanism involves transient, thermally driven unwrapping and rewinding of the DNA ends from the octamer surface (5,6). Such breathing motions provide dynamic accessibility for wrapped DNA sequences close to the entry/exit region, but the sequences buried deep within the wound DNA remain inaccessible. For providing accessibility to buried sequences, other mechanisms have evolved. These involve sliding of nucleosomes from one location to another along the DNA and partial/complete eviction of the histone octamers, which are generally carried out by specialized

ATP-consuming protein complexes called chromatin remodelers (7,8).

The intermolecular interactions between DNA and the histones undoubtedly play a critical role in regulating DNA accessibility. Strong interactions are required to overcome the bending stiffness of DNA and wrap it into its eventual superhelical conformation found in nucleosomes. Such strong binding is provided by electrostatic, hydrogen-bonding, and van der Waals interactions between histone residues and DNA phosphates and bases (1,2). These interactions are concentrated within 14 distinct sites along the wound length of DNA at locations where the DNA minor groove makes contact with the histones (9). The strongest of these sites are located at the nucleosome dyad, where the L2 and L1 loops of H3 and H4, respectively, make contact with the DNA, and $\sim \pm 40$ bp from the dyad, where the L1 and L2 loops of H2A and H2B, respectively, make contact with the DNA (9,10). The presence of these three strong sites was recently confirmed by a novel single-molecule assay involving the forced unzipping of wound DNA in a single nucleosome using optical tweezers (11). These sites also seem to contribute to the pausing of the RNA polymerase as it transcribes the wound DNA on nucleosomes (12,13).

The dynamical response of nucleosomes to externally imposed forces on DNA and its relationship to the underlying histone/DNA interactions, however, is not fully understood. Such dynamics would be relevant to processes like chromatin remodeling that use forces to manipulate the wound DNA in nucleosomes. Bennink et al. (14) were the

Submitted March 15, 2012, and accepted for publication July 30, 2012.

*Correspondence: garya@ucsd.edu

Editor: David Millar.

© 2012 by the Biophysical Society
0006-3495/12/09/0989/10 \$2.00

<http://dx.doi.org/10.1016/j.bpj.2012.07.043>

first to observe the unwrapping of DNA from individual nucleosomes within nucleosome arrays stretched by optical traps. Brower-Toland et al. (10) subsequently found that nucleosomes unraveled in two steps: the outer DNA turn unwrapped spontaneously at low forces, whereas the inner turn unwrapped at high forces giving rise to a prominent rip in the force-extension plot, which has now been confirmed by others (15–17). Various physical mechanisms have been proposed to explain this difference in the unwrapping of the two turns. The original study (10) suggested that particularly strong histone/DNA interactions ± 40 bp from the dyad required large forces to dissociate, causing the outer turn to unwrap irreversibly. Kulic and Schiessel (18) proposed that the intrinsic geometry of the nucleosome in which the outer turn unwrapping is aided by the electrostatic repulsion from the inner turn (and not vice versa) is responsible for the differences in the unwrapping of the two turns. They also showed that nucleosome unraveling is accompanied by significant deformation of the linkers, which contributes strongly to the net energy barrier of unraveling. Sudhanshu et al. (19) further noted that this deformation energy increases with DNA tension. Because the inner turn unwraps at higher tensions, its energy barrier must be larger than that for the outer turn unwrapping, which takes place at smaller tensions.

Several studies have also explicitly simulated the dynamics of nucleosomes subjected to forces. Wocjan et al. (20) used a coarse-grained (CG) model of the nucleosome to examine its unraveling under dynamic loading. The study confirmed the experimentally observed reversible and irreversible release of the two turns and also provided estimates of the unraveling energy barrier. However, as the study employed uniform histone/DNA interactions across the wound length of DNA, the effects of the strong patches of histone/DNA interactions at the dyad and off-dyad locations could not be determined. Ettig et al. (21) recently carried out steered molecular dynamics simulations of an all-atom model of the nucleosome in explicit water. Though these simulations were limited to short times (100 ns) and large pulling rates (5 m/s), they yielded several new insights. Most notably, the histone tails were found to impede DNA unwrapping at different stages of the unraveling process.

Here, we introduce a CG model of the nucleosome that permits simulation of the unraveling dynamics of nucleosomes over timescales in excess of hundreds of microseconds. At the same time, this model accounts for the nonuniform histone/DNA interactions along the wound length of DNA obtained from a recent nucleosomal-DNA unzipping assay and also reproduces the unraveling forces obtained from dynamic force spectroscopy experiments. The model reveals the detailed dynamics of the DNA and the octamer during unraveling as well as the role of the nonuniform histone/DNA interactions in the unraveling process.

MODEL DEVELOPMENT

Modeling of DNA and histone octamer

Our model nucleosome is composed of 117 nm-long double-stranded DNA, 146 bp of which is wrapped 1.7 times around a histone octamer and the remaining overhangs symmetrically from the octamer (see Fig. 1 A). The DNA and the octamer are treated as distinct entities, capable of assembling and disassembling, which allows us to probe the dynamics of nucleosome unraveling. Below we provide only the essence of the model. Additional details are provided in Section S1 and Table S1 of the Supporting Material and (22,23).

The DNA is treated using the discretized worm-like bead-chain model (Fig. 1 A), where each bead represents a 3 nm segment of relaxed DNA, yielding a total of $N_{dna} = 39$ DNA beads. Each bead is assigned a salt-dependent charge q_{dna} that interacts with other DNA beads through a Debye-Hückel potential. The DNA bead-chain is also assigned an intramolecular force field composed of stretching, bending, and twisting terms that capture its mechanics.

The histone octamer is treated as a rigid body, constructed from $N_{oct} = 65$ CG beads (Fig. 1 B). The octamer carries a shallow spiral groove on its curved face that is attractive to DNA to promote its superhelical wrapping. To obtain the dimensions of this groove, a three-dimensional helix is fitted to the axis of the wrapped DNA in the 1KX5 nucleosome crystal structure (1). We define DNA axis in terms of the midpoints of lines connecting pairs of phosphates on the

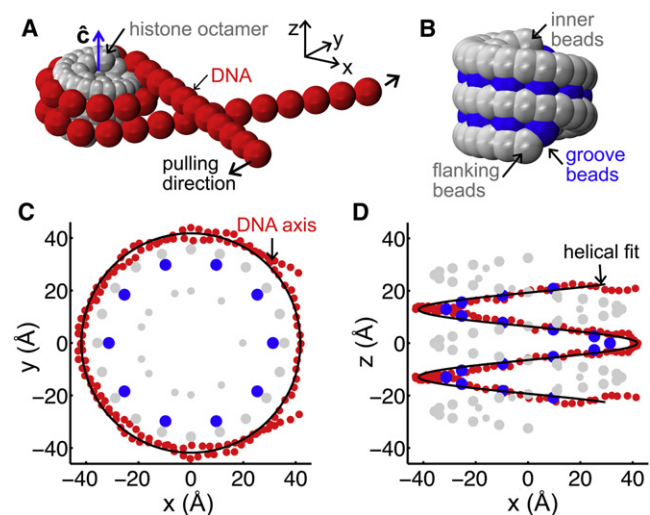


FIGURE 1 (A) CG model of the nucleosome showing the DNA (red) wrapped around histone octamer (gray). Also indicated are the pulling directions, the coordinate system, and the DNA superhelical axis \hat{c} . (B) Model of the histone octamer showing the charged, groove beads (blue) and neutral beads flanking the groove and inside the core (gray). (C and D) Cartesian coordinates of the groove (blue circles), flanking (gray circles), and inner bead helices (gray dots) that promote the wrapping of DNA in a helical path (black line) approximating the axis of wrapped DNA (red dots) in the nucleosome crystal structure.

two DNA strands involved in Watson-Crick basepairing (Fig. 1, *C* and *D*). The program PDBSUP (24) is adapted to obtain the best-fit helix passing through the DNA axis. The groove is chosen to follow a helical path with the same axis and pitch as that of the wrapped DNA determined previously but with a smaller helix diameter. We create the groove from $N_{gr} = 17$ charged beads placed equidistant from each other along this helix and additional $N_{flk} = 34$ neutral beads flanking the two sides of the groove. These flanking beads are also placed equidistant from each other along helical paths offset axially from the groove helix. Their purpose is to ensure stable wrapping of DNA around the octamer. We also introduce $N_{cen} = 14$ neutral beads in the middle to ensure that the DNA does not enter the octamer during simulations. To ensure that the DNA beads do not enter the interior of the octamer and that they do not overlap extensively with the oppositely charged groove beads, all octamer beads interact with the DNA through an excluded volume potential modeled by using the Lennard-Jones potential. In addition, the charged groove beads interact with the DNA beads using the Debye-Hückel attractive potential. This model of the octamer allows for a reasonably resolved description of the nonuniform histone/DNA interactions while keeping the number of interaction sites to a minimum.

Nucleosome unraveling simulations

We use a Brownian dynamics (BD) approach to simulate the unraveling dynamics of the nucleosome, where the two terminal linker beads are pulled at constant speeds in opposite directions along the y -direction (Fig. 1 *A*). The Supporting Material Section S2 provides a detailed description of the BD methodology and Table S1 provides the associated parameters.

Parameterization of octamer/DNA interactions

We use two different types of experimental data, collected at 150 mM monovalent salt, to parameterize the octamer groove bead charges $q_{oct,i}$. First, we use the cumulative, position (x)-dependent DNA/octamer binding free energy profile $G_{exp}(x)$ recently obtained by Forties et al. (25) to determine the relative magnitudes of $q_{oct,i}$. The free energy profile was derived by analyzing the single-molecule experiments of Hall et al. (11), where the DNA on single nucleosomes was unzipped at constant force and the time intervals, or dwell times, between the unzipping of successive basepairs were measured. Second, we use the single-molecule experiments of Pope et al. (17) that measure the average force F_{unr} termed unraveling force at which DNA unravels completely from the octamer when nucleosome arrays are stretched apart at a constant speed. These experiments indirectly provide us the net strength of histone/DNA interactions, allowing us to derive the absolute values of $q_{oct,i}$.

The $q_{oct,i}$ thus assigned represent effective charges whose Debye-Hückel attraction with the DNA beads reproduces the net effect of all types of attractive interactions between the DNA and octamer, such as ionic interactions, direct and indirect hydrogen bonds, and van der Waals contacts, which are accounted for in the experimentally measured dwell times and rupture forces.

We first derive the relative magnitudes of $q_{oct,i}$ from $G_{exp}(x)$. This profile is not symmetric about the dyad axis and has a variable resolution of 5–8 bp, which is incompatible with the fixed resolution of $\Delta x \equiv 146 \text{ bp}/N_{gr} = 8.59 \text{ bp}/\text{bead}$ required by our model. Hence, we make $G_{exp}(x)$ symmetric about the dyad and convert into a continuous function $G_{fit}(x)$ through spline fitting. We then use $G_{fit}(x)$ to derive the binding free energy contribution $\Delta G_{exp}(i)$ from each groove bead i , where $i = 1, \dots, N_{gr}$:

$$\Delta G_{exp}(i) \equiv G_{fit}(i\Delta x) - G_{fit}((i-1)\Delta x), \quad G_{fit}(0) = 0. \quad (1)$$

The above procedure is described in more detail in Section S3 and Fig. S1 of Supporting Material. Our aim is to obtain a set of $q_{oct,i}$ that would yield $\Delta G_{exp}(i)$ to within a multiplicative constant. For this purpose, we break down the total binding free energy $\Delta G_{exp} \equiv \sum_{i=1}^{N_{gr}} \Delta G_{exp}(i)$ into two contributions:

$$\Delta G_{exp} = \Delta U_{do} + \Delta G_{rem} \equiv \Delta G_{rem} + \sum_{i=1}^{N_{gr}} \Delta U_{do}(i), \quad (2)$$

where ΔU_{do} denotes position-dependent attraction between the DNA and octamer arising from salt bridges and hydrogen bonds, whereas ΔG_{rem} accounts for all remaining unfavorable position-independent contributions arising from DNA bending and DNA/DNA repulsion. Because ΔG_{rem} is independent of position, we can smear it equally over all groove beads:

$$\Delta G_{exp}(i) = \Delta U_{do}(i) + \frac{\Delta G_{rem}}{N_{gr}}. \quad (3)$$

In our model, $\Delta U_{do}(i)$ is treated by using screened electrostatic interactions whose strength is proportional to $q_{oct,i}$:

$$\Delta U_{do}(i) \approx -Kq_{oct,i}, \quad (4)$$

where $K > 0$ is a multiplicative factor enforcing attraction. We also note from our simulations that the total energy of the octamer/DNA complex is roughly half of the total electrostatic attraction between the DNA and octamer (see Fig. S2). We therefore tentatively assert that ΔG_{exp} drops down to a fraction $\alpha = 1/2$ of the total attraction ΔU_{do} due to unfavorable contributions that resist DNA wrapping, whereby

$$\Delta G_{exp} = \alpha \Delta U_{do} \equiv \alpha \sum_{i=1}^{N_{gr}} \Delta U_{do}(i). \quad (5)$$

Equations 2–5 then provide us a way to derive $q_{oct,i}$ from experimental $\Delta G_{exp}(x)$ to within a multiplicative constant (see complete derivation in Section S4 of the Supporting Material):

$$Kq_{oct,i} = -\Delta G_{exp}(i) - \frac{1-\alpha}{\alpha N_{gr}} \sum_{i=1}^{N_{gr}} \Delta G_{exp}(i). \quad (6)$$

In simple terms, the right-hand side of Eq. 6 represents a vertically shifted derivative of the cumulative free energy profile reported by Forties et al. (Fig. S1 A). Because the $q_{oct,i}$ thus obtained are relative, we can scale them for convenience to yield $q_{oct,i}^0$ such that $\sum_{i=1}^{N_{gr}} q_{oct,i}^0 / N_{gr} = 1$. Fig. 2 plots $q_{oct,i}^0$ (black squares) along the wound length of DNA relative to the dyad. The derived $q_{oct,i}^0$ distribution along the wound DNA agrees qualitatively with the number of direct and indirect hydrogen bonds (1) showing the largest number of hydrogen bonds at the dyad followed by the two off-dyad locations (Fig. S3). The charge distribution also agrees qualitatively with the histone/DNA interaction energy profile computed from all-atom simulations of nucleosomes (21), which also exhibit strongly negative energies close to the dyad and at $\sim \pm 40$ –45 bp from the dyad. For comparison, we have also plotted in Fig. 2 the scaled charge profile if all groove beads were assigned equal charge (green line) and the scaled charge profile if the ΔG_{rem} term was ignored in the charge parameterization (red circles); in this case the scaled charges is simply equal to the scaled $\Delta G_{exp}(x)$.

We next determine the absolute magnitudes of $q_{oct,i}$ that would yield the same unraveling forces F_{unr} at different

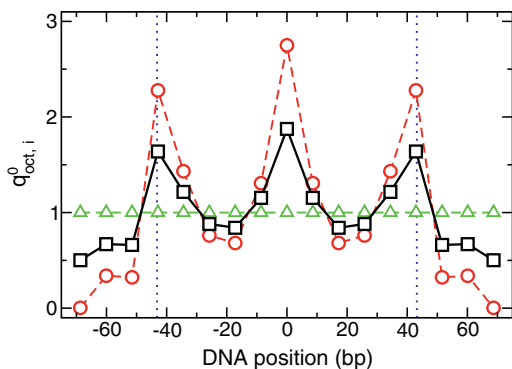


FIGURE 2 Normalized nonuniform charges $q_{oct,i}^0$ assigned to the groove beads as a function of their location along the wound length of DNA relative to the dyad (black squares), as derived from the free energy profile of Forties et al. (25). For comparison, we also show charges obtained if ΔG_{rem} were neglected (red circles) and when uniform histone/DNA interactions were implemented (green triangles). The inner turn span is indicated by dotted blue lines.

loading rates \dot{F} (rate at which the applied force increases) as those measured experimentally (17). To this end, we perform BD simulations of our model nucleosome in which the ends of the linker DNA are pulled apart at a relative speed v_{pull} . We repeat these simulations for different values of the scaling factor λ used to obtain $q_{oct,i}$ according to $q_{oct,i} = \lambda q_{oct,i}^0$. Multiple pulling speeds within the range 0.025–0.25 cm/s are employed for each λ . Note that the speeds or loading rates typically imposed in simulations are orders of magnitude higher than the ~ 10 –100 nm/s rates typically employed in the single-molecule experiments (10,15). Hence, a direct comparison between computed and experimental F_{unr} is not possible. To facilitate quantitative comparison between the two, we use a model based on Kramers' theory (26,27) for extrapolating the computed F_{unr} to small loading rates (see Section S5 of Supporting Material and Fig. S4 for details). According to this model, the average force F_{unr} at which a system subjected to a loading rate \dot{F} crosses over a transition state separating two stable states is given by

$$F_{unr} = \frac{\Delta G^*}{\nu x^*} \left[1 - \left\{ \frac{1}{\beta \Delta G^*} \ln \frac{k_0 e^{\beta \Delta G^* + \gamma}}{\beta x^* \dot{F}} \right\}^\nu \right], \quad (7)$$

where ΔG^* is the height of the energy barrier associated with unraveling, x^* is the distance between the barrier and the fully wrapped state, k_0 is the unraveling rate at zero force, $\gamma = 0.578$, $\nu = 2/3$, and $\beta = 1/k_B T$. Through an iterative procedure, we find that $\lambda = 7.1 \equiv \lambda_0$ provides a good fit between the computed and experimental F_{unr} (Fig. 3), yielding values of $\Delta G^* \approx 17.7$ kcal/mol, $x^* \approx 4.28$ nm, and $k_0 \approx 2.53 \times 10^{-6} \text{ s}^{-1}$, close to those obtained earlier (20). Hence, we set our groove charges according to $\lambda = 7.1$ for all our simulations.

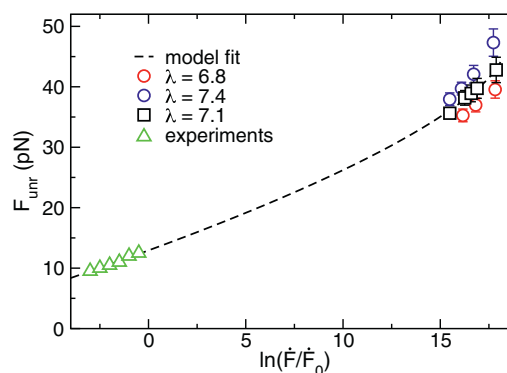


FIGURE 3 Mean unraveling force F_{unr} as a function of the normalized loading rate $\ln(\dot{F}/\dot{F}_0)$ computed for $\lambda = 6.8$ (red circle), 7.1 (black square), and 7.4 (blue circle) compared to the experimentally measured values (green triangles), where $\dot{F}_0 = 1$ pN/s. $\lambda = 7.1$ yields the best match between simulations and experiments. The dashed line represents the best fit of the simulated and experimental F_{unr} via Eq. 7. The data for $\lambda = 6.8$, 7.1, and 7.4 correspond to simulations performed with $v_{pull} = 0.05, 0.1, \text{ and } 0.25$ cm/s; 0.025, 0.05, 0.075, 0.1, and 0.25 cm/s; and 0.025, 0.05, 0.1 cm/s, and 0.25, respectively.

RESULTS AND DISCUSSION

We first investigate the forced unraveling of canonical nucleosomes possessing nonuniform histone/DNA interactions (*black squares*, Fig. 2), where groove beads carry charges given by $q_{oct,i} = 7.1q_{oct,i}^0$. We then investigate the role of nonuniform histone/DNA interactions by comparing results from canonical nucleosomes with those obtained for noncanonical nucleosomes possessing uniform histone/DNA interactions, where all groove beads carry a fixed charge of $+7.1e$ such that the net charge is the same as that of the canonical nucleosome (*green triangles*, Fig. 2). The BD simulations involve pulling the two linker ends apart with equal and opposite speeds of $v_{pull}/2$, starting from the crossed-linker configuration of Fig. 1 A, until the nucleosomes have unraveled and the linker ends are >120 nm apart. We employ five different pulling speeds v_{pull} in the range 0.025–0.25 cm/s, with the simulations spanning 20–400 μ s. To obtain reliable averages, we perform 36 simulations for each pulling speed. Because all pulling speeds yielded similar unraveling behavior, we present only the results from one pulling speed; results from two other pulling speeds are provided in Fig. S5 and Fig. S6.

Force-extension behavior

Fig. 4 A presents the force-extension behavior of canonical nucleosomes for $v_{pull} = 0.05$ cm/s. The computed force-extension plots show good qualitative agreement with those measured experimentally for mononucleosomes and nucleosome arrays; see, for example, Fig. 1 C of (10) and Fig. 4 A of (16). In particular, all plots exhibit a prolonged,

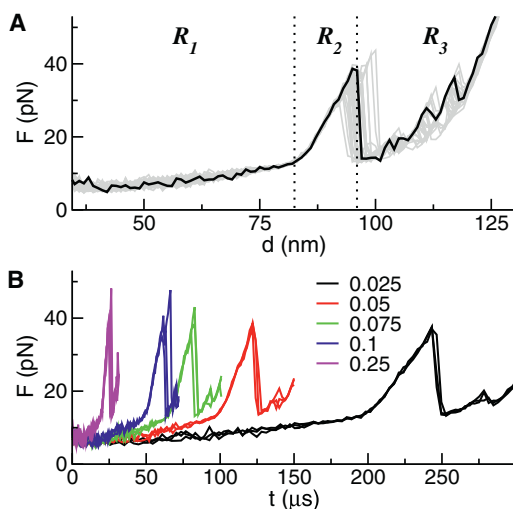


FIGURE 4 (A) Computed force-extension curves for pulling speed $v_{pull} = 0.05$ cm/s. One representative curve is shown in black, whereas the remaining 35 are shown in gray. (B) Representative force-time curves (3 each) for five different pulling velocities: $v = 0.025$ (black), 0.05 (red), 0.075 (green), 0.1 (blue), and 0.25 cm/s (magenta). Rough locations of the three unraveling regimes are also indicated.

gradual rise in force in the initial stages of pulling until an extension $d \sim 79\text{--}83$ nm or a force of 10 pN has been reached. We denote this regime of slow force growth by \mathcal{R}_1 . The gradual rise in force gives way to a steep, near-linear rise in the force culminating in a sudden drop or rip in the plots at $d \sim 100$ nm. We denote this regime of sharp force growth by \mathcal{R}_2 . The sudden drop in force at the end of \mathcal{R}_2 signifies nucleosome unraveling, whereupon most of the DNA dissociates from the octamer. After unraveling, the force begins to rise again in a sharp, nonlinear manner with respect to extension, resembling the stretching of naked DNA. We denote this regime of sharp drop and rise in force by \mathcal{R}_3 . The evolution of the total energy of the nucleosome and its components during unraveling are discussed in Section S6 of Supporting Material and Fig. S2.

Fig. 4 B presents representative force-time plots for all five pulling speeds investigated here. The average force at which the nucleosome unravels F_{unr} increases with v_{pull} and is plotted in Fig. 3. This increasing trend is common to most microscopic transitions that involve thermal crossing of an activation energy barrier, where the application of a stretching force results in the tilting of the energy landscape and an effective lowering of the energy barrier. Faster pulling leads to higher dissipation, and consequently a larger force to unravel nucleosomes. This observed increase in F_{unr} with v_{pull} is also consistent with the existing theoretical models discussed earlier (26,27).

DNA unwrapping dynamics

We characterize the dynamics of DNA unwrapping in terms of the time evolution of the number of turns n_{wrap} of DNA wrapped around the histone octamer, where $n_{wrap} = 1.7$ and 0 represent fully wrapped and unwrapped nucleosomes, respectively. Fig. 5 A shows representative $n_{wrap}(t)$ profiles computed from BD simulations performed

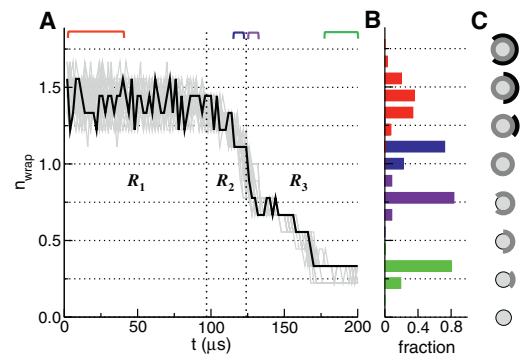


FIGURE 5 (A) Time evolution of the extent of nucleosome wrapping $n_{wrap}(t)$ for $v_{pull} = 0.05$ cm/s. A representative trajectory is shown in black, whereas the remaining 35 trajectories are shown in gray. (B) Frequency histograms of $n_{wrap}(t)$ obtained before reaching 50 nm extension (red), immediately before the rip (blue), immediately after the rip (violet), and well after the rip (green). (C) Schematics of the wrapped state of the nucleosome; the inner and outer turns are shown in gray and black, respectively.

with $v_{pull} = 0.05$ cm/s. Fig. 5 B plots the distributions in n_{wrap} at four distinct points during unraveling: initial portion of \mathcal{R}_1 with $d < 50$ nm; end of \mathcal{R}_2 within a 6 μ s time-window preceding the force rip; beginning of \mathcal{R}_3 within a 4 μ s window following the rip; and later portion of \mathcal{R}_3 for $d > 115$ nm when the DNA is taut again. The distributions are obtained by averaging over 36 simulations performed at the specified pulling speed. Note that the computed n_{wrap} has a resolution of ~ 0.111 turns due to the discrete nature of our DNA.

Figs. 5 A shows that the wrapped DNA close to the entry/exit site comes on and off the surface of the octamer within regime \mathcal{R}_1 . In particular, n_{wrap} fluctuates between a partially wrapped state containing ≈ 1.22 turns and a fully wrapped state with ≈ 1.67 turns (Fig. 5 B, red distribution), which corresponds to ~ 20 bp of DNA coming on and off the octamer surface from each end. The unwrapping and rewrapping dynamics likely arise due to weak histone/DNA interactions at these flanking portions of wound DNA (see Fig. 2). These breathing motions are believed to make wrapped DNA sequences close to the entry/exit site accessible to protein binding (5,6) and are well supported by fluorescence resonance energy transfer measurements on mononucleosomes (28,29). Apart from these breathing motions, we do not observe any major unwrapping of DNA in \mathcal{R}_1 . This dynamic nature of the entry/exit region also underscores the importance of linker histone binding for stapling together the entering and exiting linkers to enable chromatin to adopt compact conformations (30).

The flanking portions of wound DNA, which fluctuate between wrapped and unwrapped states in \mathcal{R}_1 , become permanently unwrapped within regime \mathcal{R}_2 due to the increasing tension within the DNA, which suppresses rewrapping (Fig. 5 A). We observe further unwrapping of DNA from both ends in this regime until $n_{wrap} \approx 1.08$ (Fig. 5 B, blue distribution), at which point the nucleosome unravels abruptly. This gradual unwrapping of ~ 0.6 turns of DNA (outer turn) within \mathcal{R}_2 is not associated with any visible rips in the force-extension plots, suggesting that it occurs near reversibly. Such reversible unwrapping of the outer turn of DNA is in agreement with previous single-molecule pulling studies (10,15–17).

The abrupt unwrapping of the nucleosome at the onset of \mathcal{R}_3 releases on average ~ 30 bp of the inner turn of DNA until $n_{wrap} \approx 0.78$ (Fig. 5 B, violet distribution). Interestingly, this unwrapping coincides with the unwrapping of DNA from the strong off-dyad patch of histone/DNA interactions, as discussed in detail below. The DNA released from the octamer takes time to become taut upon further pulling before the force-extension curves begin to rise sharply. In this part of \mathcal{R}_3 , additional DNA gets unwrapped (reversibly). The DNA however does not dissociate completely from the octamer, even with extended pulling. Instead, $n_{wrap} \approx 0.22$ – 0.33 turns or 20–30 bp of DNA

remains attached to the octamer, mostly (in $\sim 83\%$ of our simulations) at the dyad location where the DNA/octamer interactions are the strongest (Fig. 5 B, green distribution). This effect might be useful to chromatin remodeling, as it allows parts of the octamer to remain associated with their destined locations on the genome, even while the nucleosome is getting disrupted during processes like transcription and replication.

Kinematics of nucleosome unraveling

The translational motion of the octamer is characterized using the Cartesian coordinates $\mathbf{r}_{cm} \equiv (x_{cm}, y_{cm}, z_{cm})$ of its center of mass. Fig. 6, A–C, shows trajectories of $x_{cm}(t)$, $y_{cm}(t)$, and $z_{cm}(t)$ from simulations performed with $v_{pull} = 0.05$ cm/s and Fig. 6, E–I, shows snapshots of the nucleosome taken at different time points along the representative trajectory shown in black in Fig. 6, A–C. During \mathcal{R}_1 , the nucleosome moves in the $+x$ -direction toward the force axis (Fig. 6, A and F); recall that $\mathbf{r}_{cm} = (0, 0, 0)$ at $t = 0$ and that the force is applied along the $\hat{\mathbf{e}}_y$ axis passing through $(24, 0, 0)$. This translational motion prevents any major buildup of tension within the linkers, explaining why the force rises so gradually in this regime (Fig. 4 A). Because the linkers remain slack, we note significant Brownian fluctuations in the octamer within \mathcal{R}_1 (Fig. 6, B and C). After sufficient pulling, the linkers become taut (Fig. 6 G), which signals the onset of \mathcal{R}_2 . In this regime, the tension in the linkers cannot relax through translation, leading to a rapid buildup of force (Fig. 4 A) and a concomitant suppression in Brownian fluctuations of the octamer

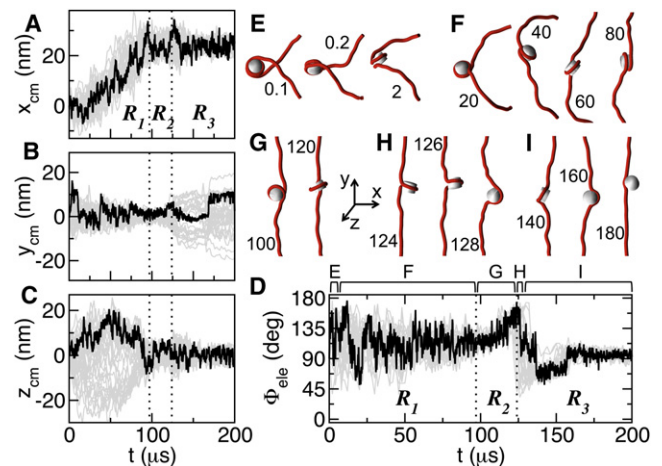


FIGURE 6 (A–C) Cartesian coordinates (x_{cm}, y_{cm}, z_{cm}) of the octamer and (D) its elevation angle Φ_{ele} as a function of time for $v_{pull} = 0.05$ cm/s. In A–D, one representative trajectory is shown in black and the remaining 35 trajectories are shown in gray. (E–I) Snapshots of the nucleosome captured at five different stages (times indicated in μ s) during the unraveling process indicated in D. In the snapshots, the DNA is shown as red cylindrical tubes spline fitted through the DNA beads and the nucleosome is shown as a gray cylinder.

(Fig. 6, B and C). Note that the deflections in the y -position of the octamer (Fig. 6 B) do not arise from Brownian motion but from an asymmetric unwrapping of DNA from its two ends. Within \mathcal{R}_3 , the Brownian fluctuations escalate upon nucleosome unraveling, as the DNA becomes slack (Fig. 6 H), but decrease with continued pulling of the linkers, as the DNA becomes taut again. The final spread in the y -position of the octamer occurs due to the sliding of the octamer along the taut DNA (Fig. 6 I).

We have analyzed the rotational motion of the nucleosome in terms of an elevation angle Φ_{ele} , defined as the angle made by the DNA superhelical axis \hat{c} and the pulling axis \hat{e}_y (Fig. 1). The azimuthal angle made by \hat{c} along the x - z plane exhibits chaotic behavior and does not reveal any meaningful trends. Fig. 6 D plots Φ_{ele} as a function of pulling time for $v_{pull} = 0.05$ cm/s; at the start of the simulation, $\Phi_{ele} = 90^\circ$ (Fig. 1 A). The strong electrostatic repulsion between the crossed linkers forces the octamer to immediately flip until its superhelical axis is almost antiparallel to \hat{e}_y and $\Phi_{ele} \sim 180^\circ$, resulting in more open linker conformations (Fig. 6 E). As the linkers are pulled apart, they impose a small torque to the octamer, gradually rotating it by another $\sim 90^\circ$ to an orientation with $\Phi_{ele} \sim 90^\circ$ (Fig. 6 F). Both these flipping events occur within the low-force \mathcal{R}_1 regime. Once the linkers have become taut in \mathcal{R}_2 , the octamer gradually begins to tilt toward an antiparallel orientation with respect to the force axis (Fig. 6 G). The taut linkers also importantly permit the nucleosome to swivel in the azimuthal direction about the pulling axis, rotating the nucleosome into orientations more amenable to unwrapping. At the point of inner turn unwrapping, the nucleosome is oriented with its superhelical axis roughly antiparallel to \hat{e}_y with $\Phi_{ele} \sim 180^\circ$, which provides the most favorable orientation for the DNA to rip off the octamer groove (Fig. 6 H). After unraveling, the octamer flips one last time (Fig. 6 I) before it comes to rest parallel to the pulling axis with $\Phi_{ele} \sim 90^\circ$.

The deterministic rotations described above are accompanied by significant fluctuations in Φ_{ele} arising from Brownian motion. A rough timescale τ_{rot} of these fluctuations may be obtained from the rotational diffusivity D_{rot} of the nucleosome via the Stokes-Einstein-Debye relation (31):

$$\tau_{rot} \sim \frac{\pi^2}{D_{rot}}; D_{rot} \approx \frac{k_B T}{8\pi\eta R^3}, \quad (8)$$

where η is the solvent viscosity and $R \approx 5$ nm is the hydrodynamic radius of a nucleosome (23). We obtain $\tau_{rot} \sim 10$ μ s, indicating that the nucleosome undergoes 10–100 random rotations during the entire unraveling process spanning 200 μ s for $v_{pull} = 0.05$ cm/s. Faster pulling speeds accommodate a lesser number of Brownian fluctuations, making it easier to distinguish deterministic from random rotations.

Role of nonuniform histone/DNA interactions

To investigate the role of nonuniform histone/DNA interactions on nucleosome unraveling, we have repeated the BD pulling simulations for noncanonical nucleosomes in which all octamer groove beads carry the same fixed charge. A comparison of the force-extension behavior and unraveling mechanism of canonical versus noncanonical nucleosomes reveals several important insights.

The noncanonical nucleosomes exhibit similar force-extension behavior as the canonical nucleosomes (Fig. 7 A), namely, the slow rise in force at small extensions; the sharp rise in force at intermediate extensions; and the sharp drop and eventual rise in force at longer extensions. Thus, the strong histone/DNA interactions at the dyad and the two off-dyad locations appear not to be responsible for the reversible and irreversible unwrapping of the outer and inner DNA turns, respectively, as suggested earlier (18,19). However, the nonuniform histone/DNA interactions do contribute to the stability of the wound DNA against extensional forces. This effect can be gleaned from Fig. 7 B, which shows consistently lower unraveling forces F_{unr} for noncanonical nucleosomes compared to canonical nucleosomes at all loading rates \dot{F} investigated here. To obtain the intrinsic energy barrier and the unraveling rates for the noncanonical nucleosome, we fit the computed $F_{unr} - \dot{F}$ data to Eq. 7. However, obtaining a good fit is challenging as the computed F_{unr} span less than two orders of magnitude in loading rates. To circumvent this, we include in the fit the experimental F_{unr} data for canonical nucleosomes at small

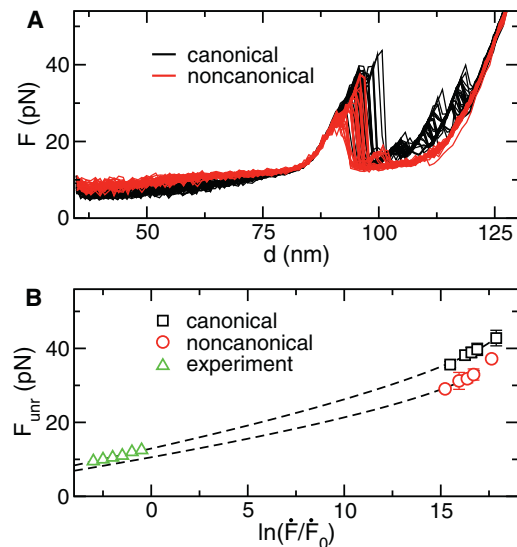


FIGURE 7 (A) Representative force-extension plots of canonical (black) and noncanonical (red) nucleosomes for $v_{pull} = 0.05$ cm/s. (B) Unraveling forces F_{unr} computed for canonical (black squares) and noncanonical (red circles) nucleosomes as a function of the normalized loading rate. The experimental data are shown as green triangles. The dashed lines represent model fits for the two data via Eq. 7.

loading rates (green triangles) multiplied by the ratio of the computed F_{unr} for noncanonical and canonical nucleosomes at large loading rates ($= 0.83$). Our rough fitting procedure yields an energy barrier of $\Delta G^* \approx 17.4$ kcal/mol located at $x^* \approx 5.20$ nm and an intrinsic unraveling rate of $k_0 \approx 3.78 \times 10^{-6} \text{ s}^{-1}$. Recalling that the canonical nucleosome yielded $k_0 \approx 2.53 \times 10^{-6} \text{ s}^{-1}$ implies that the nonuniform histone/DNA interactions lead to a 1.5-fold inhibition in the intrinsic unraveling rate of nucleosomes.

The evolution of n_{wrap} with time (Fig. 8 A) and its distributions (Fig. 8 B) at distinct points during unraveling reveal critical differences in the unwrapping dynamics of the two types of nucleosomes. First, the noncanonical nucleosome remains almost fully wrapped during \mathcal{R}_1 , with $n_{wrap} \approx 1.7$ on average, and the flanking DNA exhibits minimal breathing dynamics, as evidenced by the narrow n_{wrap} distribution (Fig. 8 B). This behavior is in stark contrast to that of the canonical nucleosomes, which exhibit $n_{wrap} \approx 1.45$ on average during the same regime and exhibit strong fluctuations in n_{wrap} , indicative of flanking DNA coming on and off the octamer surface (Fig. 8, A and B). Thus, the particularly weak histone/DNA interactions near the entry/exit regions of regular nucleosomes between 50 and 73 bp (Fig. 2) facilitates breathing dynamics so critical for protein/DNA binding. Second, the noncanonical nucleosome undergoes earlier unwrapping of the inner turn, at $n_{wrap} \approx 1.22$, compared to its canonical counterpart that undergoes un-

wrapping at $n_{wrap} \approx 1.11$. As a result, the noncanonical nucleosome releases a larger length of DNA during this transition, ≈ 35 bp, corresponding to the 0.41-turn decrease in n_{wrap} ; compare this to ≈ 26 bp of DNA released by canonical nucleosomes (Fig. 8 B). Given that the two off-dyad patches of strong histone/DNA interactions span $n_{wrap} = 0.69\text{--}1.10$ (Fig. 2) suggests that these patches are responsible for the observed delay in the unraveling of canonical nucleosome from 1.22 to 1.1 turn, i.e., DNA unwrapping pauses upon hitting the two patches, requiring a large buildup of force to rip the DNA off the octamer at these sites.

The noncanonical nucleosomes exhibit similar albeit gentler flipping motions compared to noncanonical nucleosomes (Fig. 8 C). In particular, the noncanonical nucleosomes unravel in a more tilted orientation with respect to the pulling direction ($\Phi_{ele} \rightarrow 135^\circ$), as opposed to canonical nucleosomes that orient more antiparallel ($\Phi_{ele} \rightarrow 180^\circ$) before unraveling (Fig. 8 C, inset). This difference arises due to the noncanonical nucleosome unraveling with 1.22 turns of wound DNA, which yields a large moment arm and thereby a large torque, causing the octamer to tilt. In contrast, the canonical nucleosomes unravel with slightly more than one turn of wound DNA, which results in a small moment arm and thereby a negligible torque, causing the octamer superhelical axis to orient antiparallel to the pulling axis.

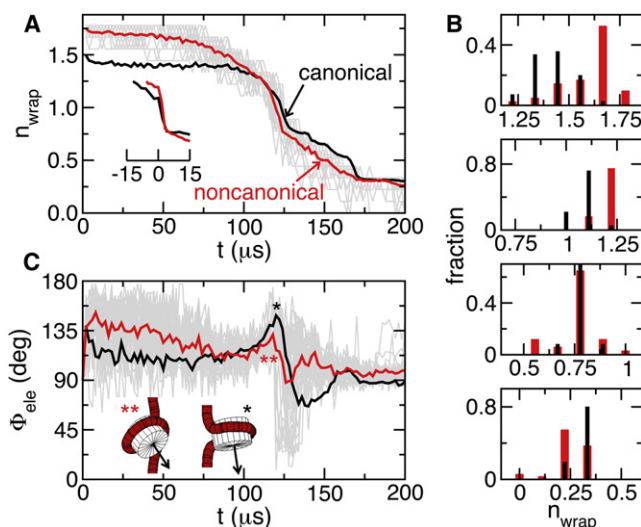


FIGURE 8 Comparison of (A) DNA unwrapping dynamics n_{wrap} and (C) octamer orientation Φ_{ele} for canonical and noncanonical nucleosomes. The individual traces from 36 simulations for noncanonical nucleosomes are shown in gray and the averages from 36 canonical and noncanonical nucleosome simulations are shown in red and black. The inset in A shows the average $n_{wrap}(t)$ for the two nucleosomes, where the individual $n_{wrap}(t)$ traces have been shifted relative to the time of inner turn unraveling (force rip). The axes scale are identical to A. The inset in C shows the orientation of the two nucleosome types at the onset of the force rip. (B) Distribution in over the same time windows as in Fig. 5 for canonical (black) and noncanonical (red) nucleosomes.

CONCLUSIONS

We have introduced a CG model of the nucleosome in which the DNA and the histone octamer are treated as separate entities capable of assembling and disassembling. In particular, the DNA is treated using a discrete worm-like chain model that accounts for DNA electrostatics and mechanics. The octamer is treated as a rigid body with a shallow groove that wraps DNA in the same left-handed superhelical conformation as in the nucleosome crystal structure. The most important and unique feature of this model is its parameterization of octamer/DNA interactions based on two different single-molecule measurements: unzipping of nucleosomal DNA, which provides us the position-dependent free energy of DNA unwrapping from histone octamers, and dynamic force spectroscopy of nucleosomes, which provides us the mean forces at which nucleosomes unravel as a function of loading rates.

This model allows us to probe via Brownian dynamics simulations the detailed dynamics of nucleosome unraveling in response to its linker ends being pulled apart at constant speed. Our simulations reveal that the nucleosome unravels in three stages. At small extensions, the force rises gradually with extension due to the nucleosome approaching the pulling axis, which keeps the linkers relaxed. The wound DNA close to the entry/exit region undergoes spontaneous unwrapping-rewrapping dynamics. Apart from

exhibiting strong Brownian fluctuations, the octamer undergoes a fast $\sim 90^\circ$ flip due to electrostatic repulsion between the crossing linkers, followed by a slow $\sim 90^\circ$ flip due to the torque imposed by the linkers. The octamer aligns with its superhelical axis perpendicular to the pulling axis. At intermediate extensions, the force rises sharply with extension, as the linkers become taut and aligned along the pulling axis. The taut linkers permit swiveling of the octamer and suppress its Brownian motion orthogonal to the pulling axis. The rising force causes a gradual, reversible release of the outer turn until about a turn of DNA remains wrapped. The octamer also undergoes a slow $\sim 90^\circ$ flip until its superhelical axis is aligned parallel to the pulling direction. At large extensions, a portion of the inner turn unwraps in an irreversible manner, signified by a rip in the force-extension plot and a $>90^\circ$ flip of the octamer. The remaining inner turn unwraps reversibly until ~ 20 – 30 bp of DNA remains attached to the octamer mostly at the dyad, which cannot be dislodged even upon extended pulling. The octamer rotates further to assume its final parallel orientation relative to the pulling direction.

The model also provides insights into the role of nonuniform histone/DNA interactions on nucleosome stability and dynamics, by comparing its unraveling characteristics to that of a noncanonical nucleosome designed to have uniform histone/DNA interactions across the wound length of DNA. First, the weak interactions near the entry/exit region of canonical nucleosomes are responsible for the unwrapping-rewrapping dynamics of the flanking portions of wound DNA, as noncanonical nucleosomes with stronger interactions in this region remain largely wrapped and exhibit less breathing motions. Second, the nonuniform histone/DNA interactions serve to stabilize the nucleosome from unraveling, as evidenced by the consistently lower unraveling forces measured for noncanonical nucleosomes. This stabilization is apparently brought about by the two off-dyad patches of strong histone/DNA interactions, which strengthen the innermost portions of the outer turn and delay the unwrapping of the inner turn. Third, both nucleosome types display abrupt unwrapping of the inner turn suggesting that the two patches of strong interactions appear not to be responsible for the abrupt unwrapping of the inner turn.

These differences in DNA unwrapping for nucleosomes with distinct histone/DNA interaction free energy profiles lead to the possibility that histone posttranslational modifications at the histone/DNA interface, which undoubtedly alter the free energy landscape of histone/DNA interactions, might be used to modulate the accessibility of wound DNA or the dissociation of octamers from DNA. In fact, Simon et al. (32) have recently demonstrated that the acetylation of Lys-56 on H3 at the entry/exit site and of Lys-79 on H4 near the off-dyad interaction patch facilitates DNA unwrapping and transcription factor binding, whereas the acetylation of Lys-115 and 122 on H3 at the dyad

interaction patch affect the complete disassembly of the nucleosome.

In conclusion, the model developed here could be extended to examine other biophysical issues in nucleosome biology, such as the propagation of DNA twist along nucleosomal DNA; the effects of core histone modifications on the breathing dynamics and stability of wrapped DNA; and the unraveling of nucleosomes within longer arrays.

SUPPORTING MATERIAL

Six sections, a table, six figures, and references (33–36) are available at [http://www.biophysj.org/biophysj/supplemental/S0006-3495\(12\)00856-9](http://www.biophysj.org/biophysj/supplemental/S0006-3495(12)00856-9).

We thank the Chancellors Interdisciplinary Collaboratories Program at University of California, San Diego for partial funding of this work and Dr. Doug Smith for discussions.

REFERENCES

1. Davey, C. A., D. F. Sargent, ..., T. J. Richmond. 2002. Solvent mediated interactions in the structure of the nucleosome core particle at 1.9 Å resolution. *J. Mol. Biol.* 319:1097–1113.
2. Luger, K., A. W. Mäder, ..., T. J. Richmond. 1997. Crystal structure of the nucleosome core particle at 2.8 Å resolution. *Nature.* 389:251–260.
3. Felsenfeld, G., and M. Groudine. 2003. Controlling the double helix. *Nature.* 421:448–453.
4. Arya, G., A. Maitra, and S. A. Grigoryev. 2010. A structural perspective on the where, how, why, and what of nucleosome positioning. *J. Biomol. Struct. Dyn.* 27:803–820.
5. Polach, K. J., and J. Widom. 1996. A model for the cooperative binding of eukaryotic regulatory proteins to nucleosomal target sites. *J. Mol. Biol.* 258:800–812.
6. Felsenfeld, G. 1996. Chromatin unfolds. *Cell.* 86:13–19.
7. Cairns, B. R. 2007. Chromatin remodeling: insights and intrigue from single-molecule studies. *Nat. Struct. Mol. Biol.* 14:989–996.
8. Bowman, G. D. 2010. Mechanisms of ATP-dependent nucleosome sliding. *Curr. Opin. Struct. Biol.* 20:73–81.
9. Luger, K., and T. J. Richmond. 1998. DNA binding within the nucleosome core. *Curr. Opin. Struct. Biol.* 8:33–40.
10. Brower-Toland, B. D., C. L. Smith, ..., M. D. Wang. 2002. Mechanical disruption of individual nucleosomes reveals a reversible multistage release of DNA. *Proc. Natl. Acad. Sci. USA.* 99:1960–1965.
11. Hall, M. A., A. Shundrovsky, ..., M. D. Wang. 2009. High-resolution dynamic mapping of histone-DNA interactions in a nucleosome. *Nat. Struct. Mol. Biol.* 16:124–129.
12. Studitsky, V. M., D. J. Clark, and G. Felsenfeld. 1995. Overcoming a nucleosomal barrier to transcription. *Cell.* 83:19–27.
13. Jin, J., L. Bai, ..., M. D. Wang. 2010. Synergistic action of RNA polymerases in overcoming the nucleosomal barrier. *Nat. Struct. Mol. Biol.* 17:745–753.
14. Bennink, M. L., S. H. Leuba, ..., J. Greve. 2001. Unfolding individual nucleosomes by stretching single chromatin fibers with optical tweezers. *Nat. Struct. Biol.* 8:606–610.
15. Gemmen, G. J., R. Sim, ..., D. E. Smith. 2005. Forced unraveling of nucleosomes assembled on heterogeneous DNA using core histones, NAP-1, and ACF. *J. Mol. Biol.* 351:89–99.
16. Mihardja, S., A. J. Spakowitz, ..., C. Bustamante. 2006. Effect of force on mononucleosomal dynamics. *Proc. Natl. Acad. Sci. USA.* 103:15871–15876.

17. Pope, L. H., M. L. Bennink, ..., J. F. Marko. 2005. Single chromatin fiber stretching reveals physically distinct populations of disassembly events. *Biophys. J.* 88:3572–3583.
18. Kulić, I. M., and H. Schiessel. 2004. DNA spools under tension. *Phys. Rev. Lett.* 92:228101.
19. Sudhanshu, B., S. Mihardja, ..., A. J. Spakowitz. 2011. Tension-dependent structural deformation alters single-molecule transition kinetics. *Proc. Natl. Acad. Sci. USA.* 108:1885–1890.
20. Wocjan, T., K. Klenin, and J. Langowski. 2009. Brownian dynamics simulation of DNA unrolling from the nucleosome. *J. Phys. Chem. B.* 113:2639–2646.
21. Ettig, R., N. Kepper, ..., K. Rippe. 2011. Dissecting DNA-histone interactions in the nucleosome by molecular dynamics simulations of DNA unwrapping. *Biophys. J.* 101:1999–2008.
22. Dobrovolskaia, I. V., M. Kenward, and G. Arya. 2010. Twist propagation in dinucleosome arrays. *Biophys. J.* 99:3355–3364.
23. Arya, G., Q. Zhang, and T. Schlick. 2006. Flexible histone tails in a new mesoscopic oligonucleosome model. *Biophys. J.* 91:133–150.
24. Rupp, B., and S. Parkin. 1996. PDBSUP: A Fortran Program that Determines the Rotation Matrix and Translation Vector for Best Fit Superposition of Two PDB Files by Solving the Quaternion Eigenvalue Problem. Lawrence Livermore National Laboratory, Livermore, CA.
25. Forties, R. A., J. A. North, ..., R. Bundschuh. 2011. A quantitative model of nucleosome dynamics. *Nucleic Acids Res.* 39:8306–8313.
26. Dudko, O. K., G. Hummer, and A. Szabo. 2006. Intrinsic rates and activation free energies from single-molecule pulling experiments. *Phys. Rev. Lett.* 96:108101.
27. Maitra, A., and G. Arya. 2010. Model accounting for the effects of pulling-device stiffness in the analyses of single-molecule force measurements. *Phys. Rev. Lett.* 104:108301.
28. Tomschik, M., H. Zheng, ..., S. H. Leuba. 2005. Fast, long-range, reversible conformational fluctuations in nucleosomes revealed by single-pair fluorescence resonance energy transfer. *Proc. Natl. Acad. Sci. USA.* 102:3278–3283.
29. Gansen, A., A. Valeri, ..., C. A. Seidel. 2009. Nucleosome disassembly intermediates characterized by single-molecule FRET. *Proc. Natl. Acad. Sci. USA.* 106:15308–15313.
30. Grigoryev, S. A., G. Arya, ..., T. Schlick. 2009. Evidence for heteromorphous chromatin fibers from analysis of nucleosome interactions. *Proc. Natl. Acad. Sci. USA.* 106:13317–13322.
31. Koenderink, G. H., and A. P. Philipse. 2000. Rotational and translational self-diffusion in colloidal sphere suspensions and the applicability of generalized Stokes-Einstein relations. *Langmuir.* 16:5631–5638.
32. Simon, M., J. A. North, ..., M. G. Poirier. 2011. Histone fold modifications control nucleosome unwrapping and disassembly. *Proc. Natl. Acad. Sci. USA.* 108:12711–12716.
33. Stigter, D. 1977. Interactions of highly charged colloidal cylinders with applications to double-stranded. *Biopolymers.* 16:1435–1448.
34. Iniesta, A., and J. G. de la Torre. 1990. A 2nd-order algorithm for the simulation of the Brownian dynamics of macromolecular models. *J. Chem. Phys.* 92:2015–2018.
35. Arya, G., and T. Schlick. 2009. A tale of tails: how histone tails mediate chromatin compaction in different salt and linker histone environments. *J. Phys. Chem. A.* 113:4045–4059.
36. Maitra, A., and G. Arya. 2011. Influence of pulling handles and device stiffness in single-molecule force spectroscopy. *Phys. Chem. Chem. Phys.* 13:1836–1842.